The Journal of Chemical Physics

Modeling state-selective photodetachment in cold ion traps: Rotational state "crowding" in small anions

Cite as: J. Chem. Phys. **151**, 144304 (2019); https://doi.org/10.1063/1.5123218
Submitted: 03 August 2019 . Accepted: 16 September 2019 . Published Online: 10 October 2019

F. A. Gianturco, L. González-Sánchez, B. P. Mant, and R. Wester

The Journal of Chemical Physics ARTICLE scitation.org/journal/jcp

Modeling state-selective photodetachment in cold ion traps: Rotational state "crowding" in small anions

Cite as: J. Chem. Phys. 151, 144304 (2019); doi: 10.1063/1.5123218
Submitted: 3 August 2019 • Accepted: 16 September 2019 •
Published Online: 10 October 2019

F. A. Gianturco,[1,a)] L. González-Sánchez,[2] B. P. Mant,[1] and R. Wester[1]

AFFILIATIONS

[1] Institut fuer Ionenphysik und Angewandte Physik, Universitaet Innsbruck, Technikerstr. 25, A-6020 Innsbruck, Austria
[2] Departamento de Química Física, University of Salamanca, Plaza de los Caídos sn, 37008 Salamanca, Spain

[a)] **Electronic mail:** Francesco.gianturco@uibk.ac.at

ABSTRACT

Using accurate *ab initio* calculations of the interaction forces, we employ a quantum mechanical description of the collisional state-changing processes that occur in a cold ion trap with He as a buffer gas. We generate the corresponding inelastic rates for rotational transitions involving three simple molecular anions $OH^-(^1\Sigma)$, $MgH^-(^1\Sigma)$, and $C_2H^-(^1\Sigma)$ colliding with the helium atoms of the trap. We show that the rotational constants of these molecular anions are such that within the low-temperature regimes of a cold ion trap (up to about 50 K), a different proportion of molecular states are significantly populated when loading helium as a buffer gas in the trap. By varying the trap operating conditions, population equilibrium at the relevant range of temperatures is reached within different time scales. In the modeling of the photodetachment experiments, we analyze the effects of varying the chosen values for photodetachment rates as well as the laser photon fluxes. Additionally, the changing of the collision dynamics under different buffer gas densities is examined and the best operating conditions, for the different anions, for yielding higher populations of specific rotational states within the ion traps are extracted. The present modeling thus illustrates possible preparation of the trap conditions for carrying out more efficiently state-selected experiments with the trapped anions.

I. INTRODUCTION

Cooling and controlling molecular ions has been an important topic for many years, owing to the importance of cold molecules for many applications such as precision spectroscopy and metrology,[1–3] quantum-state controlled chemistry,[4,5] or laboratory astophysics.[6–8] Available techniques for the preparation of molecular ions in specific quantum states of vibrational or rotational motion and in selected hyperfine states are photoionization of suitable precursors[9] or buffer gas cooling.[10] Optical pumping[11,12] or depletion of excited states[13] have also been demonstrated. Most of these techniques rely on a sufficiently large spacing between different quantum states, for example, spacings substantially larger than the relevant thermal energies. However, for heavier diatomics or for polyatomic molecular ions, this becomes increasingly difficult to provide.

A widely used approach to internally cool molecular ions is based on using cryogenic ion traps, where ion samples are trapped and cooled down to a few kelvin with the use of buffer gas that fills the trap.[10,14] Helium is commonly used for this purpose to thermalize internal degrees of freedom to a temperature near the buffer gas temperature. In radiofrequency ion traps, the de-excitation of rotational quantum states has been demonstrated for several systems.[13,15] The lowest temperature achievable for helium buffer gas is about 4 K, which leads to molecular ions with rotational temperatures near this limit. In the present study, we shall provide a computational model of the kinetics of photodetachment of several negative ions from selected initial states, simulating trap conditions with temperatures between 4 K and 30 K.

In experiments, preparation of trapped molecular anions in a selected set of rovibrational states usually starts by loading internally hot ions, with state distributions determined by the production

process, into the ion trap. Excited rovibrational levels then cool by interaction with the buffer gas or by direct radiative emission. Time scales depend on the inelastic scattering rate coefficients and the dipole moments of radiative transitions.[16] For most small anions, vibrational excitation is completely quenched, while the population of the rotational states is controlled by the buffer gas temperature and the collisional state-changing rates. During the rotational quenching collisions, the anions' excitation energy is redistributed as kinetic energy between both collisional partners. Most molecular anions studied in traps are heavier than the helium atoms of the buffer gas so that the latter carry most of the kinetic energy released after the state-changing collisions. Elastic collisions with the buffer gas atoms reduce the translational velocities of the trapped anions to a temperature near that of the He atoms.

The photodetachment processes of interest here will be interpreted as causing transitions between the molecular anion, M^-, in its ground electronic state and the neutral molecule, M, also in its ground electronic state. Near threshold, both the neutral molecule produced and the initial anion are considered in their vibrational ground state but in different rotational states depending on the photon energy.[17] In the case of a linear molecule, one can write

$$M^-(J') + h\nu \rightarrow M(J'') + E_{kin}. \quad (1)$$

The final rotational state of the neutral follows definite transition selection rules which depend on J' and also on the initial and final electronic states of the partners.[13] By ensuring that the laser frequency neutralizes only molecular anions that are above a certain rotational level in the ion trap, one can perform state-selective photodetachment experiments that produce specific final states of the anions left in the trap[13,18] and allow for preparation of the absolute internal ground state of a specifically selected molecular anion's rotational state.

The aim of the present work is to analyze in detail the quantum formulation of experimental processes where specific molecular anions will be initially produced in their lower rotational states by collisions with He buffer gas and then allowed to equilibrate their

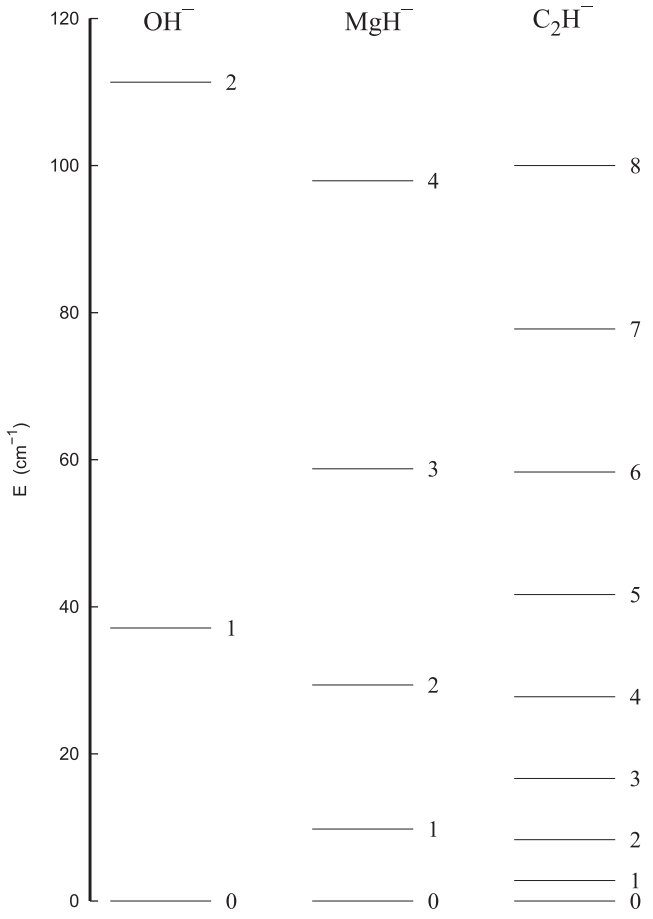

FIG. 1. Computed rotational levels for the lower levels of $OH^-(^1\Sigma)$, $MgH^-(^1\Sigma)$, and $C_2H^-(^1\Sigma)$ covering a range of about 120 cm^{-1}. The B_{rot} values are taken from the references quoted in the main text.

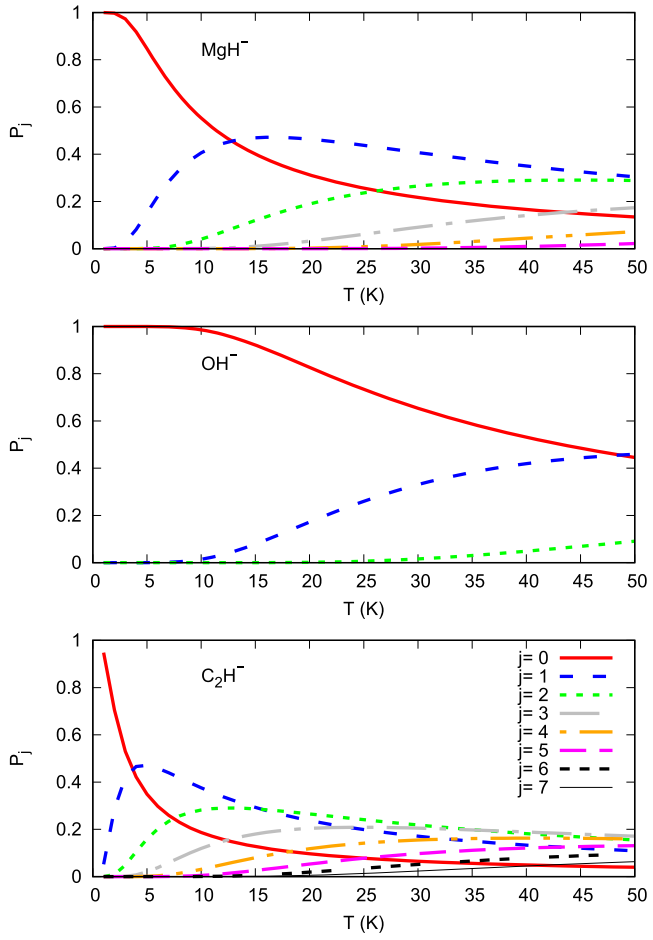

FIG. 2. Computed rotational level populations as a function of trap temperature. The three panels contain data for the $OH^-(^1\Sigma)$ anion, for the $MgH^-(^1\Sigma)$ molecular anion, and for the $C_2H^-(^1\Sigma)$ anion.

rotational temperatures with the gas temperature in the trap. They will then be exposed to laser light of a specific frequency that will only depopulate some preselected rotational states of anions. The population losses in the trap will depend on the structure of the anion under consideration, the physical nature of their interaction with the He buffer gas, and the interplay between the collisional density of the uploaded gas and the photon flux of the neutralizing laser. These two dynamical paths will therefore be the main agents in the interplay of ion losses and collisional repopulation.

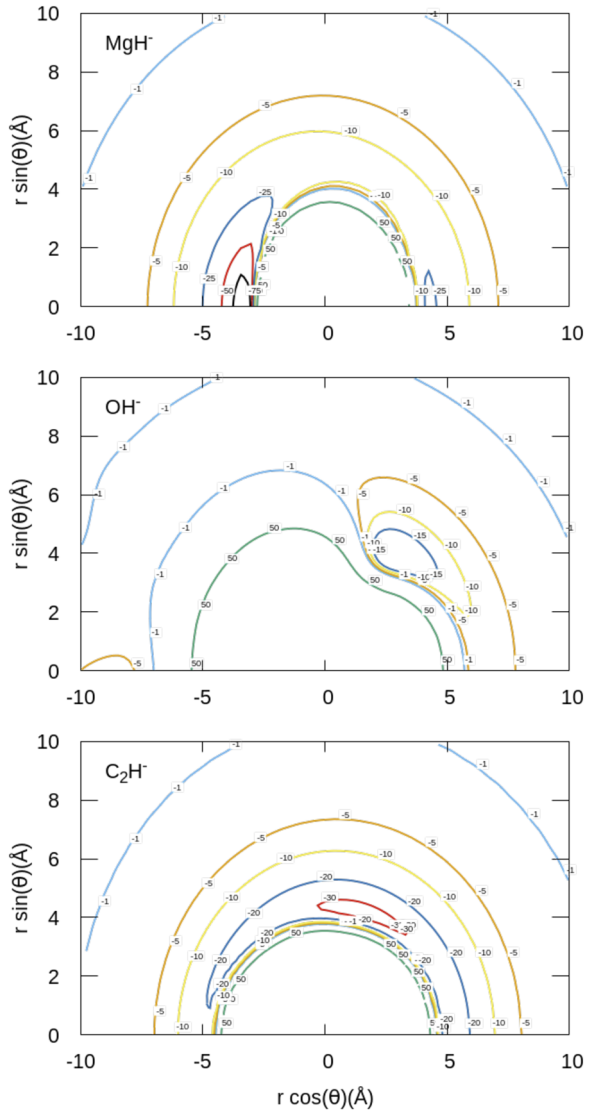

FIG. 3. Energy maps associated with the three PESs employed in the present work involving the rigid-rotor interactions of $MgH^-(^1\Sigma)$ (top panel), $OH^-(^1\Sigma)$ (middle panel), and $C_2H^-(^1\Sigma)$ (bottom panel) with a He atom. Distances are in Å, and interaction energy is in cm^{-1}. The maps presented here are adapted from Ref. 22 (top panel), Ref. 19 (middle panel), and Ref. 21 (bottom panel). See main text for further details.

The paper is organized as follows. Section II will briefly summarize the nature of the interaction forces between the selected anions and the He buffer gas atoms and discuss the internal rotational structures of the anions. In Sec. III, we will describe the collisional equilibration of the ions with the helium gas at the trap temperature and solve the ensuing kinetics equations. In Sec. IV, we will examine the rates of spontaneous emission of photons in the ion trap but show this to be a negligible consideration. In Sec. V, we present calculations for the different thermalization time scales for each anion in the traps. In Sec. VI, we will show the effect of switching on the neutralizing laser on the anions' population losses from specific rotational states of the anion in question. Finally, we offer conclusions in Sec. VII.

II. ROTATIONAL STRUCTURES AND INTERACTION POTENTIALS

In this section, we shall describe in some detail the structural properties of the simple anionic molecules we will analyze. More

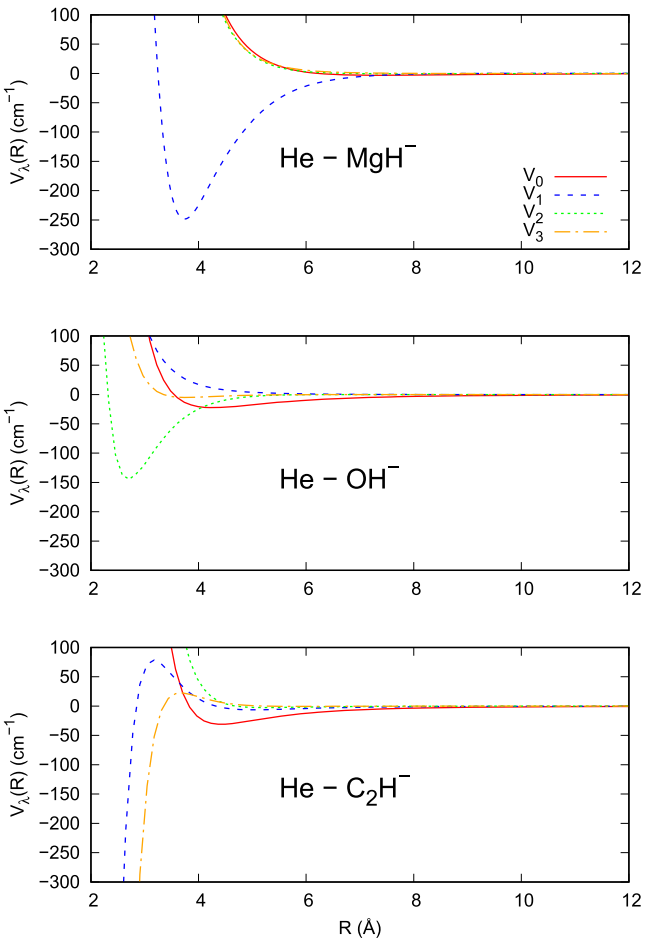

FIG. 4. Computed radial coefficients of the expansion in Eq. (2) for the three molecular anions interacting with He. Only the first four most important radial functions are given in each case.

specifically, we shall show how the densities of rotational states per unit energy change drastically from $OH^-(^1\Sigma^+)$ to $MgH^-(^1\Sigma^+)$ and to $C_2H^-(^1\Sigma^+)$ and how such changes are also linked to differences between their potential energy surfaces (PESs) describing their interaction with He, the buffer gas of choice in the cold traps where the photodetachment experiments are carried out.

The rotational constants, B_0, for each of these molecules have been presented before: 18.570 cm^{-1} for OH^- in Ref. 19, 4.897 cm^{-1} for MgH^- in Ref. 20, and 1.389 cm^{-1} for C_2H^- in Ref. 21.

Figure 1 shows a comparison between the energy spacings of the lower rotational levels for the three molecules under consideration.

It is interesting to note how markedly the densities of the rotational states vary within the energy range of about 100 cm^{-1} from one molecule to the next: OH^- essentially has two rotational levels in the range, which become five for MgH^- and about eight for C_2H^-. This means that their preparation in a cold ion trap will provide us with different significant populations of their rotational states as a function of the trap temperature. For a direct comparison between these systems, we present in Fig. 2 the relative Boltzmann populations over a range of 0–50 K for OH^-, MgH^-, and C_2H^-.

The results of the equilibrium population shown in that figure clearly indicate that one should expect the OH^- anion to be present, after thermalization, in chiefly its $j = 0$ and $j = 1$ rotational states. On the other hand, rotational states up to about $j = 4$ are populated for MgH^- at around 30 K, while from Fig. 2 it can be seen that in the case of C_2H^- molecules will significantly be populated up to $j = 6$ or 7 states at 30 K. Thus, we can expect that the trapping of these anions in cold ion traps will allow them to be present with very different populations of their lower rotational states.

As discussed in the Introduction, rotational/vibrational cooling of the trapped anions is carried out by loading helium as a buffer gas at different densities. Thus, after thermalization to the $v = 0$ vibrational states of the molecular ions, further collisional cooling to their internal rotational states will be achieved over a finite time scale by collisional interactions with He atoms. The interaction forces for the molecular anions with He atoms have been obtained from accurate *ab initio* calculations and analyzed in previous publications: $OH^-(^1\Sigma)$ has been presented in our earlier work in Ref. 19 and further employed in the calculations of Ref. 13. The corresponding *ab initio* potential energy surface for $MgH^-(^1\Sigma)$ interacting with He has also been computed by us earlier, and its features, quality of treatment, and other details have already been presented in Ref. 22. Finally, the rigid-rotor (RR) potential describing the interaction of $C_2H^-(^1\Sigma)$ anions with He has been calculated to a high level of accuracy by Dumouchel *et al.* in Ref. 21, and we shall not repeat here the details of that calculation.

A pictorial comparison between these three PESs is shown in Fig. 3 where we show the interaction energy in units of cm^{-1} for all three molecules as a function of the Jacobi coordinates (r, θ) expressed as Cartesian variables $(r\cos\theta, r\sin\theta)$. The molecules are fixed at their respective equilibrium bond lengths as described in the relevant references given above.

The data presented in Fig. 3 give some further insight into the differences between the three PESs of this study. The excess negative charge present in all three molecules makes their interaction with the closed-shell He atom rather repulsive from all directions, with only a fairly limited cone of approach where attractive interactions are present. For the case of $C_2H^-(^1\Sigma)$, for instance, the weakly attractive well appears off-axis and in the direction of the C–H bond, while for $MgH^-(^1\Sigma)$ the well is placed along the molecular axis, on the side of the Mg atom as already discussed in some detail in Ref. 22. The $OH^-(^1\Sigma)$ target also shows an off-axis approach as the one containing the attractive well, directed toward the middle of the O–H bond.

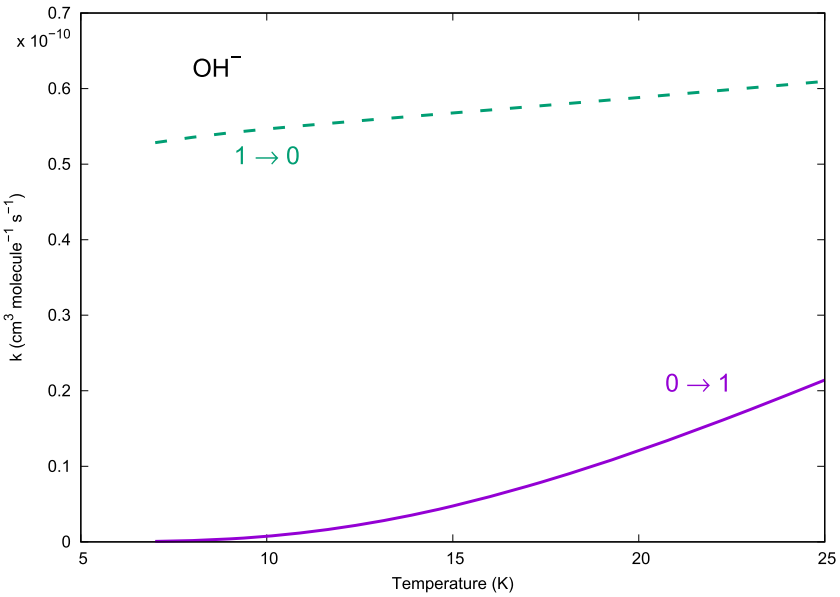

FIG. 5. Computed rotationally inelastic collisional rates at low temperatures for OH^-. See main text for further details.

Another useful presentation of the anisotropic features of the present PESs is obtained by expanding the rigid-rotor, two-dimensional (2D) potentials in a series of Legendre polynomials,

$$V(r_{\rm eq}|R,\theta) = \sum_{\lambda}^{\lambda_{\rm max}} V_\lambda(r_{\rm eq}|R) P_\lambda(\cos\theta). \quad (2)$$

The radial shapes of the lower terms of the sum in Eq. (2) are shown in the three panels of Fig. 4, where the interaction energy is in units of $\rm cm^{-1}$ and distances are in angstrom. All three molecules are kept at their equilibrium geometries.

It is interesting to note that the three systems exhibit different anisotropic features of their expansion coefficients. The top panel in Fig. 4 for the MgH^- case indicates that the $\lambda = 1$ coefficient has the strongest attractive well, thereby suggesting that the direct dynamical coupling between rotational levels with a $\Delta j = \pm 1$ difference will be the strongest in this system. This also occurs for the OH^- anion, as shown in the middle panel of Fig. 4, although in this case the attractive well of the $V_\lambda(r_{\rm eq}|R)$ coefficients is closer to the molecule and weaker than that of the MgH^- case. One therefore expects once again that inelastic rotational state-changing collisions will be favored for processes with $\Delta j = \pm 1$ as a selection rule.

The case of the triatomic anion C_2H^- shown in the bottom panel of Fig. 4 indicates an overall much stronger angular anisotropy for this system. The V_2 and V_3 coefficients are strongly attractive, while the V_0 and V_1 terms behave in the opposite way. Therefore

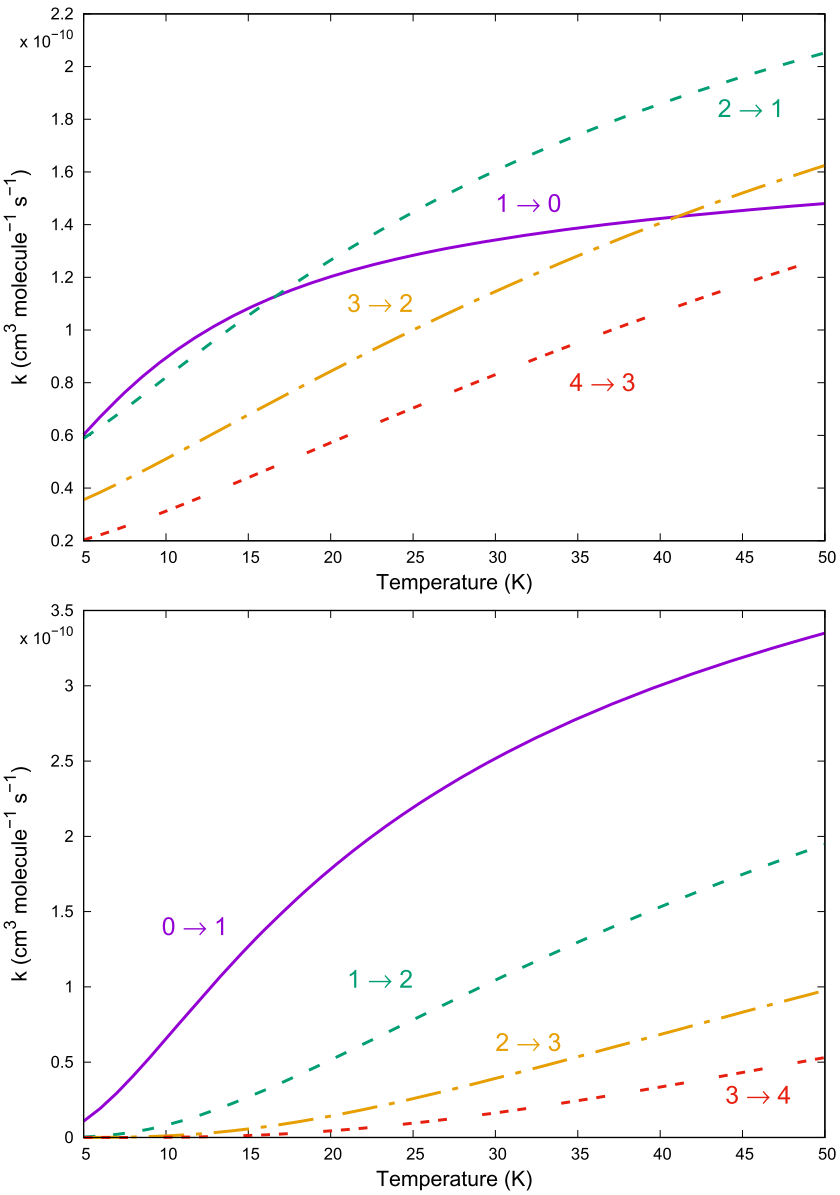

FIG. 6. Computed state-changing collisional rates for MgH^- in ion traps with He as a buffer gas. The upper panel shows de-excitation ("cooling") rates, while the lower panel reports the excitation ("heating") rates over the same range of temperatures. See main text for comments.

(and as shown below), we expect different Δj values to participate efficiently in coupling rotational levels during inelastic collisions with the He buffer gas. Such aspects will be briefly discussed in Sec. III for all three molecular targets.

III. STATE-CHANGING QUANTUM DYNAMICS

Solving the problem of rotational quenching dynamics corresponds to solving the time-independent Schrödinger equation (TISE) for the nuclei that move on the potential energy surfaces discussed in Sec. II, defined by Eq. (2) and enforcing on their motion the usual asymptotic scattering boundary conditions.[23]

Our numerical strategy to solve the TISE is the coupled channel (CC) approach as implemented in our in-house developed scattering code, ASPIN.[24] Details of the method have been given before[25,26] and discussed recently in detail for the case of the para-H_2^+–He system[27] and so will not be reported here.

It is worth noting that for the present systems, all angular momentum couplings are fully accounted for by our CC description of the nuclear dynamics and hence the calculation of the rotational quenching process given by our computational model can be considered as basically exact, within the accuracy of the employed PES.

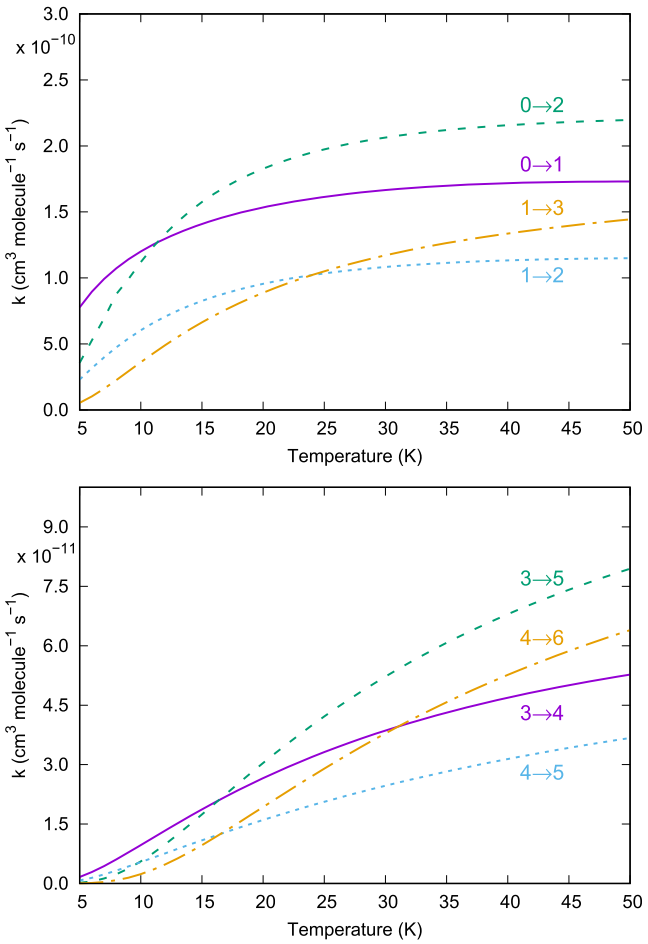

FIG. 7. Computed rotational excitation rates for the C_2H^- anion for temperatures up to 50 K in the trap. The upper panel shows transitions involving the lowest three levels, while the lower panel shows excitation rates from higher rotational levels.

TABLE I. Computed state-changing collisional rates for MgH^- at T = 15 K.

i	j	k_{ij}(cm^3 s^{-1})
0	1	1.27×10^{-10}
0	2	9.80×10^{-12}
1	0	1.08×10^{-10}
1	2	2.68×10^{-10}
2	0	3.28×10^{-11}
2	1	1.05×10^{-10}
2	3	5.67×10^{-12}
3	2	6.78×10^{-11}
3	4	1.32×10^{-12}
4	3	4.40×10^{-11}

The molecular basis set consists of about 30 rotational functions for each of the target ions that have been used in the asymptotic channel expansions. A detailed discussion of an earlier calculation for the C_2H^-–He system has been given to which we refer the reader for more information.[21]

The $\sigma^J_{j_i \to j_f}(E)$ partial integral cross sections have been carefully checked for convergence with the basis set size and propagator parameters and are converged to within 1%. In particular, we have propagated the solution from R = 1.0 Å to at least R = 50.0 Å with 500 steps of the LogDer propagator.[16] The convergence of the sums of the partial cross sections to obtain the corresponding state-to-state integral cross sections was also controlled by extending the total angular momentum J value up to at least $J_{max} = 80$.

As we want to describe the rotational quenching process, we are principally interested in the (de-)excitation transition cross sections between different rotational states within the same vibrational level: $(v_0, j = j_i) \to (v_0, j = j_f)$ with v_0 indicating the vibrational ground state of the target anion. For the sake of notational clarity, in the following formulas, we assume implicitly that the system is always in its vibrational ground state, v_0.

Once the integral cross sections are known, the rotationally inelastic rate constants $k_{j \to j'}(T)$ can be evaluated as the convolution of the computed inelastic cross sections over a Boltzmann distribution of the relative collision energies. In the equation below, all quantities are given in atomic units,

TABLE II. Computed state-changing collisional rates for OH^- at T = 15 K.

i	j	k_{ij}(cm^3 s^{-1})
0	1	4.75×10^{-12}
1	0	5.68×10^{-11}
1	2	1.00×10^{-12}
2	0	2.20×10^{-12}

$$k_{j\to j'}(T) = \left(\frac{8}{\pi\mu k_B^3 T^3}\right)^{1/2} \int_0^\infty E\sigma_{j\to j'}(E) e^{-E/k_B T} dE. \quad (3)$$

We report in Fig. 5 examples of the behavior of the rotational excitation rates for the OH^- target over a range of temperatures up to 25 K. It is clear from the data that the OH^- rates involve chiefly the first two excited rotational states.

A greater range of temperatures and of inelastic processes are shown for the MgH^- anion in the two panels of Fig. 6 in order to further assess this different behavior with respect to OH^-. One can clearly see from these calculations that both excitation ("heating") and de-excitation ("cooling") state-changing collisional rates are fairly large and are comparable in size over a larger range of rotational states than is the case for OH^-, where essentially only the first two levels are involved in the collisional state-changing processes.

The same calculations involving rotational levels up to $j = 6$ are reported for the C_2H^- target in the panels of Fig. 7. The calculations involve excitation rates and clearly indicate the importance of the $\Delta j = 2$ transitions in relation to the $\Delta j = 1$ processes which dominate the state-changing collisional rates for the other two systems. We further see that many more rates are now comparable in size and therefore expected to play a significant role in collisional repopulation processes in the ion traps.

To report more specifically the numerical values of the relevant rates, we show in Table I the inelastic collisional rates for MgH^- and in Table II for OH^- at a selected typical trap temperature of 15 K. Both excitation and de-excitation processes are reported.

The same results for the state-changing collisional rates for C_2H^- are given in Table III also for 15 K. Again, it can be seen how many more levels are involved with rates of comparable sizes and with a more significant level population as discussed for the bottom panel of Fig. 2 in comparison with the other panels of that figure.

TABLE III. Computed rotationally inelastic collisional rates between the lower levels of C_2H^- expected to be populated in the trap at 15 K (see discussion of Fig. 2).

i	j	$k_{ij}(\mathrm{cm}^3\ \mathrm{s}^{-1})$
0	1	1.41×10^{-10}
0	2	1.58×10^{-10}
0	3	5.10×10^{-12}
0	4	7.90×10^{-12}
1	0	6.06×10^{-11}
1	2	8.26×10^{-11}
1	3	6.64×10^{-11}
1	4	1.07×10^{-12}
1	5	1.63×10^{-12}
2	0	7.52×10^{-11}
2	0	7.52×10^{-11}
2	1	7.81×10^{-11}
2	3	3.86×10^{-11}
2	4	3.28×10^{-11}
3	0	4.24×10^{-12}
3	1	1.58×10^{-10}
3	2	7.23×10^{-11}
3	4	1.87×10^{-11}
3	5	1.74×10^{-11}
4	0	1.62×10^{-11}
4	1	4.83×10^{-12}
4	2	1.75×10^{-10}
4	3	4.43×10^{-11}
4	5	1.09×10^{-11}
4	6	9.68×10^{-12}
5	1	2.68×10^{-11}
5	2	6.18×10^{-12}
5	3	1.70×10^{-10}
5	4	3.63×10^{-11}
5	6	7.43×10^{-12}
6	1	2.16×10^{-12}
6	2	3.08×10^{-11}
6	3	8.23×10^{-12}
6	4	1.59×10^{-10}
6	5	3.37×10^{-11}

IV. INTERACTION WITH BLACK-BODY RADIATION

Another important process for characterizing the internal state distribution of the anions in the trap is their interaction with the surrounding radiative field, also known as black-body radiation. A molecule interacts with such a field by absorbing and emitting photons. The transition rates from an excited state k can be written as a sum of stimulated and spontaneous emission rates as[28]

$$\kappa^{em}_{k\to i} = \kappa^{sti}_{k\to i} + \kappa^{spo}_{k\to i} = A_{k\to i}(1 + \eta_\gamma(\nu, T)), \quad (4)$$

where $A_{k\to i}$ is the Einstein coefficient for spontaneous emission and $\eta_\gamma(\nu, T) = (e^{(h\nu/k_B T)} - 1)^{-1}$ is the Bose-Einstein photon occupation number.

The Einstein coefficient for dipole transitions is given as

$$A_{k\to i} = \frac{2}{3}\frac{\omega^3_{k\to i} S_{k\to i}}{\epsilon_0 c^3 h(2j_k + 1)}, \quad (5)$$

where $\omega_{i\to k} \approx 2B_0(j_i + 1)$ is the transition's angular frequency and $S_{k\to i}$ is the line strength, a quantity clearly linked to the Einstein coefficients via the multiplicity factors pertaining to the present processes. For pure rotational transitions, Eq. (5) simplifies to

$$A_{k\to i} = \frac{2}{3}\frac{\omega^3_{k\to i}}{\epsilon_0 c^3 h}\mu_0^2 \frac{j_k}{(2j_k + 1)}, \quad (6)$$

where μ_0 is the internuclear electric dipole moment of the molecule.

In order to verify the relative importance of the spontaneous emission process *viz-á-vis* the collisional state-changing rates discussed above, we have calculated $A_{k\to i}$ using Eq. (6) for all three molecular anions considered.

In Table IV, we compare the Einstein coefficients with corresponding computed collisional rates from Tables I–III. For this comparison, we selected a typical trap temperature of 15 K and a

TABLE IV. Computed Einstein spontaneous emission coefficients for C_2H^-, MgH^-, and OH^- [Eq. (6)] compared to collisional rates at T = 15 K. All quantities in units of s^{-1}. See main text for further details. C_2H^- μ_0 = 3.09 D,[29] MgH^- μ_0 = 1.864 D,[20] OH^- $\mu_0 \approx$ 1.0 D.[30] $\eta_{He} = 5 \times 10^{10}$ cm^{-3}.

Transition $j \to j'$	C_2H^- $A_{j\to j'}$	C_2H^- $\eta_{He} \times k_{j\to j'}$	MgH^- $A_{j\to j'}$	MgH^- $\eta_{He} \times k_{j\to j'}$	OH^- $A_{j\to j'}$	OH^- $\eta_{He} \times k_{j\to j'}$
$1 \to 0$	2.14×10^{-5}	3.03	3.41×10^{-4}	5.40	5.46×10^{-3}	2.84
$2 \to 1$	2.05×10^{-4}	3.90	3.28×10^{-4}	5.25	...	...
$3 \to 2$	7.43×10^{-4}	3.62	1.18×10^{-2}	3.39	...	...
$4 \to 3$	1.83×10^{-3}	2.21	2.91×10^{-2}	2.20	...	...
$5 \to 4$	3.65×10^{-3}	1.82	...	...	...	...
$6 \to 5$	6.40×10^{-3}	1.69	...	...	...	...

buffer gas density in the trap of 5×10^{10} cm^{-3}. The dipole moment values are also reported in Table IV.

We clearly see from the comparison that the contribution to anion losses in the cold traps from interaction with black-body radiation is negligible with respect to state changing effects caused by collisional processes under trap conditions. We can therefore safely disregard their contribution to the repopulation dynamics in the cold ion traps, which we shall describe in Sec. V.

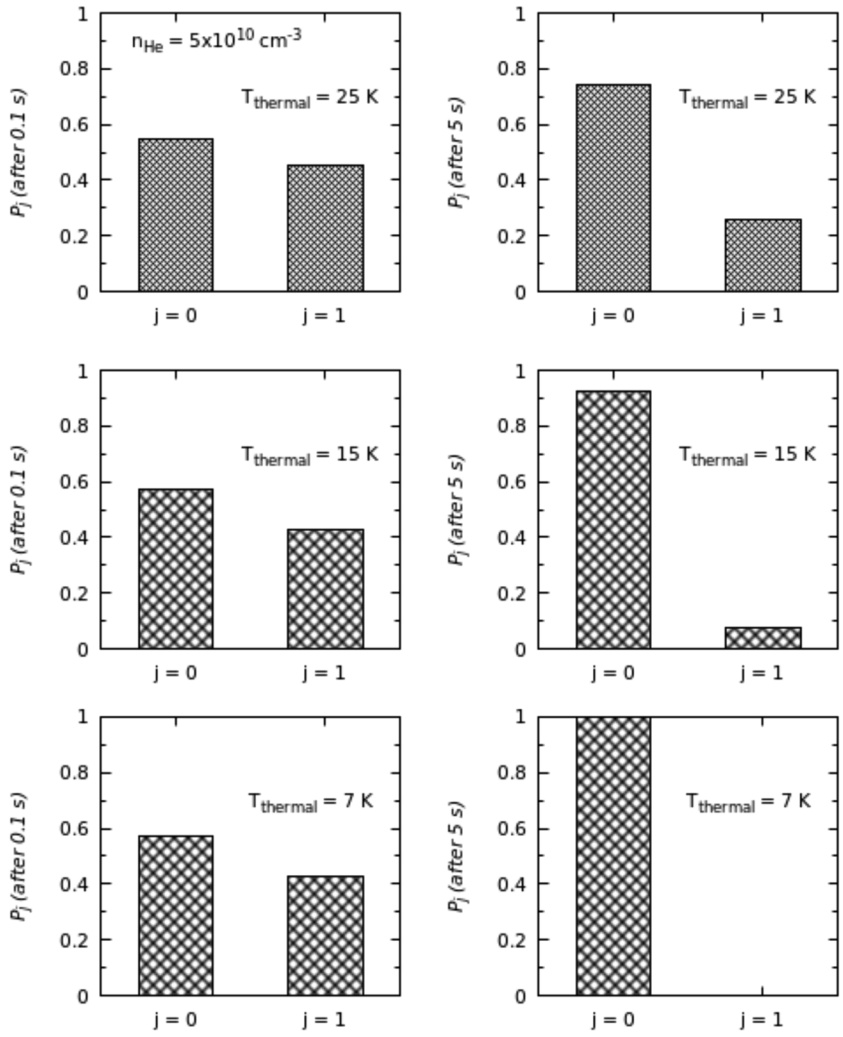

FIG. 8. Computed collisional thermalization populations of OH^- molecules at 25 K (upper panels), 15 K (middle panels), and 7 K (bottom panels) after 0.1 s (left columns) and 5 s (right columns). See main text for further details.

V. THERMALIZATION DYNAMICS

To quantitatively verify the effects of "level crowding" generated by the differences in rotational spacing between the three molecules, as shown in Fig. 1, we have carried out calculations of collisional thermalization of the three molecules at different trap temperatures, ranging from 10 K to 50 K, and a selected density of the buffer gas of 5×10^{10} cm^{-3}, over different time intervals that were shown to reach equilibrium between the molecular ions in the trap and the temperature of the buffer gas. The details of the procedure were already discussed in Ref. 27 and will not be repeated here. The results are reported for OH^- and MgH^- in the panels of Figs. 8 and 9. In each case, initial populations were those at 50 K.

The calculations of Fig. 8 indicate that OH^- is not yet thermalized with the buffer gas after 0.1 s, while after 5 s the anionic molecules have reached the Boltzmann distribution at the three temperatures considered. In all three cases, the dominant population is that of the $j = 0$ level, this being most strikingly so at the lowest temperature of 5 K.

If we now examine the behavior of the MgH^- anions given in the panels of Fig. 9, we see that thermalization is a more rapid process since the populations at the highest temperature are close to being already thermal after 0.1 s. Furthermore, the level populations clearly favor the $j = 1$ level except for the lowest temperature of 5 K.

The data regarding the C_2H^- anion are collected in Fig. 10 where thermalization is clearly fully achieved after 1.0 s (see populations in Fig. 2). The collisional redistribution among rotational levels now involves many more levels, especially at the highest temperature considered.

The analysis of the populations in the thermalized traps clearly indicates the following features:

(i) The OH^- achieves thermalization more slowly because only two levels are significant so that only their direct state changing rates can play a meaningful role.
(ii) As the level spacing decreases in going to MgH^- and C_2H^-, we see that a more "crowded" network of state-changing

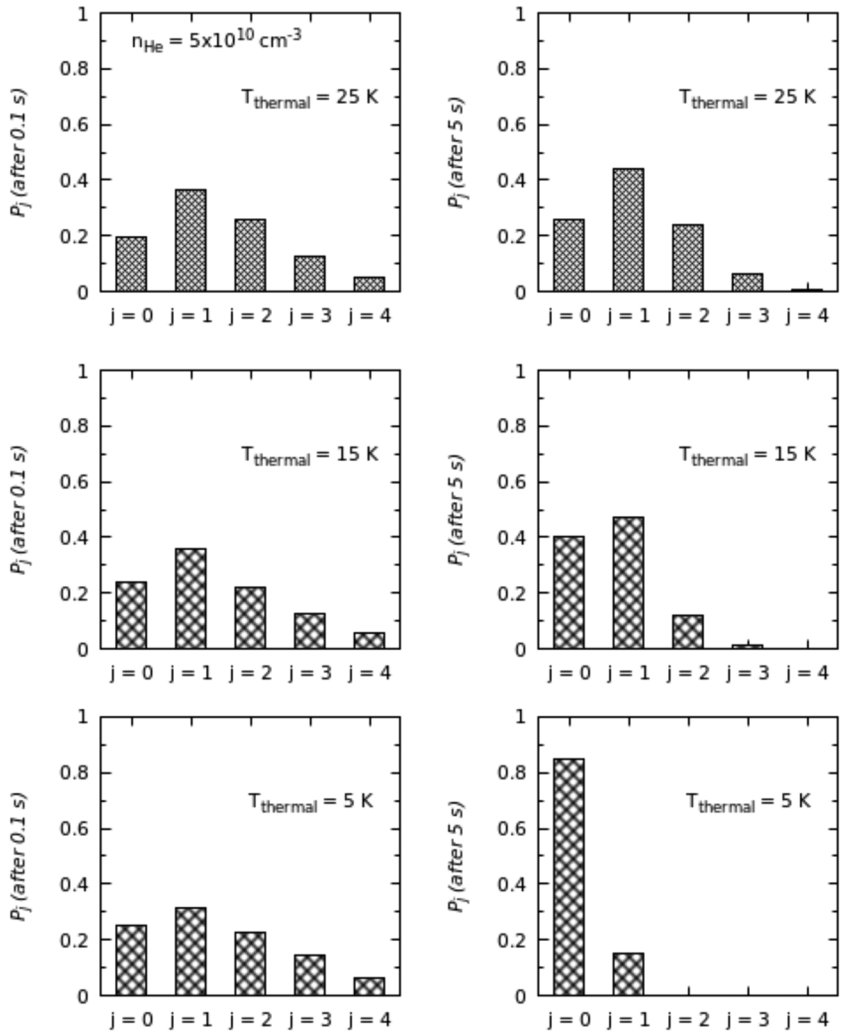

FIG. 9. Same calculation as in Fig. 8 but for MgH^-. The lowest temperature considered is 5 K, while all other conditions are as in Fig. 8.

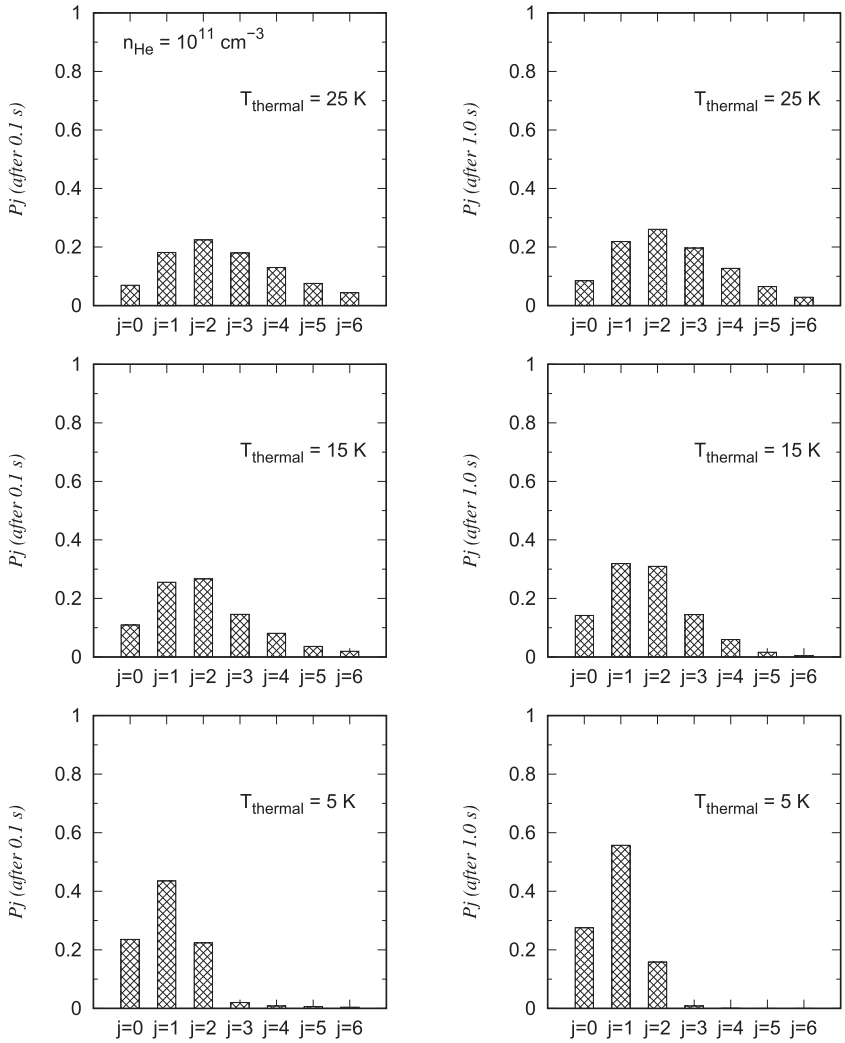

FIG. 10. Same calculations as for Figs. 8 and 9 but for C_2H^-. The populations are already thermalized with the buffer gas after 1.0 s. See main text for further details.

rates comes into play. This causes faster thermalization, and a larger number of indirect collisions play a role during level collisional repopulation.

(iii) The latter features are particularly evident for the case of C_2H^- and are bound to affect the redistribution process during photodetachment experiments.

Section VI will specifically analyze such differences with respect to state-selective electron photodetachment.

VI. DYNAMICS OF STATE-DEPENDENT PHOTODETACHMENT

As discussed in the Introduction, we wish to analyze in some detail the direct photodetachment processes for the title molecular anions after they have been loaded into a cold trap and collisionally thermalized with He atoms as the buffer gas of the present modeling. The plots reported in Figs. 11 and 12 indicate the selection rules controlling the photodetachment (PD) processes for the MgH^- and C_2H^- molecules from specific rotational levels, which are expected to be populated in the trap. The case of the OH^- anion has been discussed before[13] and will not be discussed again in this section.

We have reported in both figures the final levels of the neutral electronic states that are populated by the selection rule for a laser at threshold. When a more energetic laser is used, even higher energy final states of the neutral molecules will be populated. In both the present cases, all the molecules involved, anions and neutrals, are in Σ electronic states and therefore a simple dipole-driven selection rule applies in all the considered transitions.

To further continue the modeling of the rotational populations during the evolutionary dynamics, we solve the master equations using the collisional thermal rates obtained before at each chosen value of the trap temperature and of the selected He density,[27]

$$\frac{dn_i(t)}{dt} = \sum_{j \neq i} n_j(t) C_{ji}(T) - n_i(t) \sum_{i \neq j} P_{ij}(T). \quad (7)$$

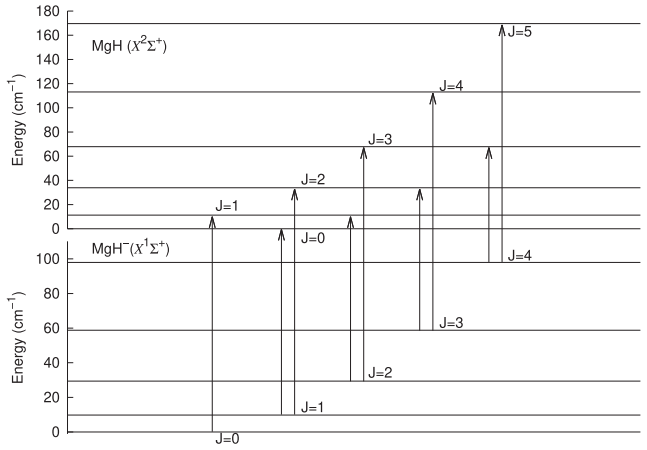

FIG. 11. Specific rotational levels of the initial molecular anion and final neutral molecule which are involved in the PD process for the MgH$^-$($^1\Sigma$) target in the ion trap. See main text for further details.

Here, $P_{ij}(T)$ are the rates for the destruction of the population of level i, while its formation rates are given by the $C_{ji}(T)$ coefficients. During the collisional step, i.e., before the laser is switched on, the coefficients are given as a function of the inelastic rate coefficients and the He density,

$$P_{ij}(T) = \eta_{\mathrm{He}} k_{i\to j}(T), \tag{8}$$

$$C_{ji}(T) = \eta_{\mathrm{He}} k_{j\to i}(T). \tag{9}$$

This describes the "collision-only" time evolution process of thermalizing the relative population of the rotational levels to the selected buffer gas temperature at a give density η_{He} in the trap. Once the thermalization process is reached and the PD laser is turned

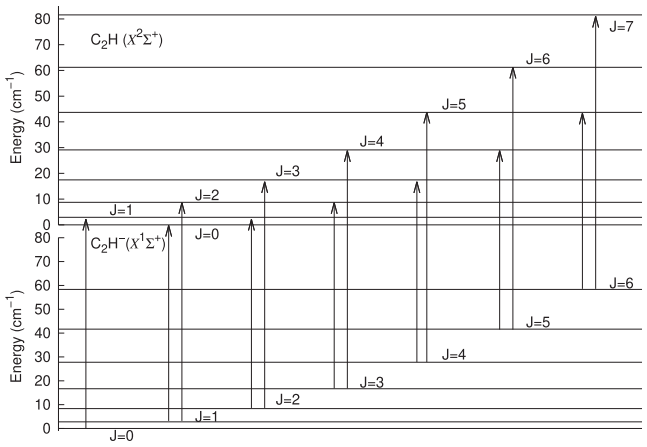

FIG. 12. Same process as those shown in Fig. 11 but for the C_2H^-($^1\Sigma$) anion in the trap. All final levels reached according to the PD selection rules are shown in the figure. See main text for further details.

on, one needs to modify the master equation (7) in the following way:

$$\frac{dn_i(t)}{dt} = \sum_{j\neq i} n_j(t) C_{ji}(T) - n_i(t)\left(\sum_{i\neq j} P_{ij}(T) + K_i^{PD}\right), \tag{10}$$

where K_i^{PD} is the additional destruction rate of the selected level i caused by the PD laser. The set of rates K_i^{PD} are critical in the experiment and for the numerical simulation because they drive the destruction of both the population of one specific rotational level i and of the molecular ions in that specific state. The absolute experimental values of the state-to-state PD cross sections at threshold are presently unknown for the MgH$^-$ and C_2H^- target molecular anions. Since the actual rates also depend on the laser photon flux and the overlap between the laser beam and the ion cloud, we shall introduce in the present calculations a global parameter α according to the relation

$$K_i^{PD} = \alpha(v)\sigma_i^{PD}(v), \tag{11}$$

where $\sigma_i^{PD}(v)$ are the (still unknown) PD cross sections for a specific rotational state of an ion (see our earlier work[31]). The modifications of the parameter α shall therefore allow us to model the changing efficiency of the PD losses of anions due to the changing intensity of the laser and to obtain the best fit between the future experimental results and the present simulation. In the following, therefore, we shall directly scale the K_i^{PD} values employed to simulate the PD processes. Because of the present lack of experimental data, for simplicity, we shall initially consider the parametrized K_i^{PD} as being independent of the rotational level i and therefore to be given as K^{PD} for all the rotational states of the anion. The possible influence of using the computed state-dependent Hoenl-London factors will be discussed in future work.

After the selected time duration of the "laser on" step, we can further analyze the population losses that can tell us, after a time t during which the laser is applied, what fraction of the ions are lost, following the previous thermalization step, due to the additional laser action on the trap's anion populations of the different rotational levels.

To better clarify the different roles of the various trap parameters, the measurement conditions can be separated into two regimes, namely, a photodetachment dominated (PD-dominated) regime and a collision-dominated regime. In the collision-dominated regime, the photodetachment rate is smaller than the inelastic collision rate with helium with the trapped anion. Here, the redistribution of the rotational levels due to inelastic collisions is faster than the ion loss rates induced by the PD laser. Thus, the population ratio stays nearly constant.

Whenever the photodetachment rate is comparable or larger than the inelastic collision rates (PD-dominated regime), the relative rotational populations are no longer in equilibrium. The first excited rotational level is thus depleted in such a way that the ion-loss rate reaches a plateau depending on the inelastic collisions of that particular anion with the helium atoms in the trap.

A numerical test of the different regimes is presented in Fig. 13 for the case of the OH$^-$–He system, which was analyzed by us in earlier work[13,19] and for which the different regimes were considered experimentally within a simple two level kinetics.[13]

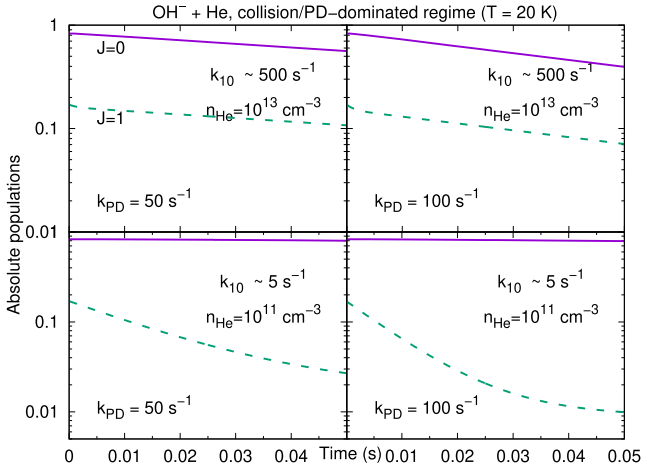

FIG. 13. Computational tests for collision-dominated and PD-dominated regimes for OH^- in a cold trap at 20 K. Two different densities for the He buffer gas are considered. See main text for details.

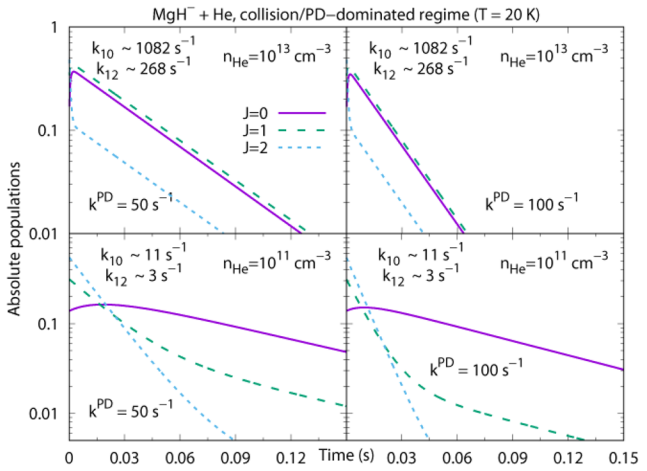

FIG. 14. Same computation as those of Fig. 13 but for the MgH^-–He system. The PD-dominated regime is shown by the lower panels, while the collision-dominated regime is shown in the upper panels. See main text for details.

The panels of Fig. 13 analyze, in the upper two panels, two different choices for the values of the parametrically chosen K^{PD} rates. Here, they are taken to correspond to fairly fast PD rates, albeit still smaller than the computed collisional rates obtained in this work. We therefore see there that the collisions with the buffer gas dominate the kinetics. The result is that the populations of the two most populated levels are kept nearly constant and no selective ion losses are observed. On the other hand, by reducing the buffer gas pressure, we show in the lower two panels the arrangement for which the PD rates become larger than the repopulation rates caused by inelastic collisions. Thus, we clearly see that the excited molecular anions which repopulate the $j = 1$ level are being emptied much faster by the PD process and rapidly leave the trap. We have used in these calculations comparatively fast PD rates to generate marked differences in the system within a shortened time interval. The experiments of Ref. 13 employed K^{PD} values between 1.0 s^{-1} and 10.0 s^{-1}. We shall test similar values in our computational models discussed below.

A similar analysis is carried out for the MgH^-–He system in Fig. 14, where we also show that there are at least two relevant state-changing rates involved and turn out, at 20 K, to be larger than those for the two main levels that are active in the case of the OH^- system of Fig. 13.

The different dynamical regimes are clearly separated in the results of Fig. 14 although we see here that the presence of more levels being populated in the MgH^- anion case complicates the relative populations and shows that the collision-dominated regime allows the identification of at least three different rotational states that remain with a constant ratio over time. By the same token, we see that the PD-dominated regime causes a selective population loss between the $j = 2$ and $j = 1$ levels, thus allowing in principle to increase the relative abundance of molecules in one level with respect to the other, thereby markedly altering the collisional repopulation conditions shown by the upper panels. We shall further discuss this specific feature of anions with closer energy spacings than in the case of OH^- in the results presented below.

An interesting comparison of collisional repopulation in the absence of laser action ($K^{PD} = 0$) and for two different trap temperatures is given by Figs. 15 and 16, where all three anions are shown at the same time. The "rotational crowding" of the involved levels, as already discussed in Fig. 1, increases from left (OH^-) to right (C_2H^-) along the molecular series.

Examining Figs. 15 and 16 leads to the following considerations:

(i) Lowering the temperature causes, as expected, a marked simplification of which are the important populations, as we move from OH^- to C_2H^-. In the latter instance in fact, several levels are significantly repopulated at 15 K, while they are reduced to the lowest three at 5 K, the same temperature for which the lowest two remain the most important in the case of MgH^-.

(ii) Increasing the collision numbers at the higher He densities clearly affects in all three cases the efficiency of the repopulation between levels. In the lower panels of both figures, their populations remain constant over the whole range of time evolution, indicating that collisional frequencies control rapid thermalization in that regime.

Once the PD laser is switched on in the simulations, such specific effects become even more evident, as shown by the data in Fig. 17.

The data in Fig. 17 show the PD process "switched on" after a time delay of 5 s. This is the time interval after which the rotational populations for all three anions have reached thermalization to the buffer gas temperature, as discussed in Sec. V. The anion losses are followed in our calculations for 10 s in the case of OH^- and for 20 s for the other two anions. The upper panels indicate different η_{He} values at a temperature of 5 K, while the lower panels examine the same situation for a buffer gas temperature of 15 K. The photodetachment rate is taken to be at a value of 1.0 s^{-1}, a typical value achieved

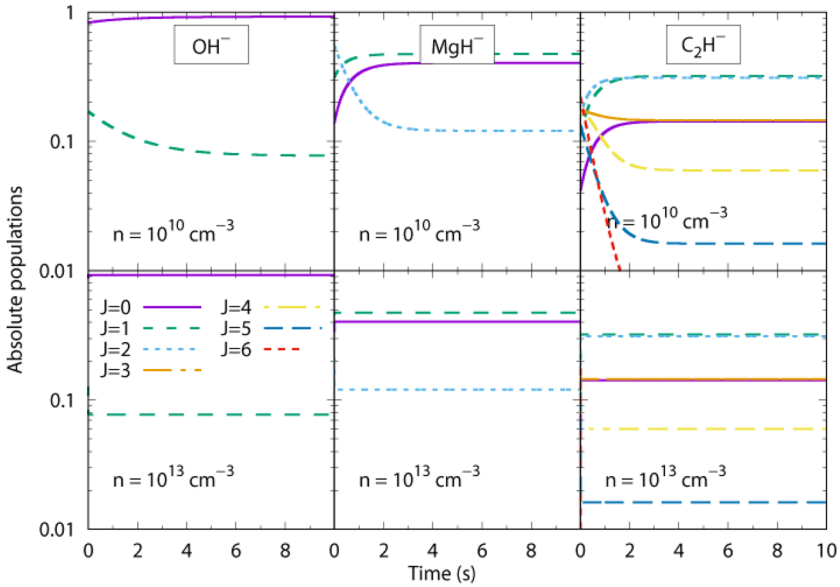

FIG. 15. Collisional population evolution at 15 K for two different choices of η_{He} values. The upper panels correspond to a low He density (10^{10} cm^{-3}), while the lower panels employ a higher He density (10^{13} cm^{-3}).

in experiments.[8,18] As mentioned earlier, this corresponds to a K^{PD} value of 1.0 s^{-1}, applied to all levels, without explicit j-dependence in it.

The simulations confirm the structural simplifications attained at the lower temperatures and for the lower densities of the buffer gas. The OH^- system shows at all conditions the rapid disappearance of anions in the $j = 1$ state, with negligible repopulation from other levels, due to their marginal population in the trap. On the other hand, low T and low η_{He} regimes for MgH^- indicate the possibility of altering the Boltzmann regimes at low T and of being able to selectively produce dominance of the $j = 0$ states of the anions. Furthermore, we see that the enlarged network of collisional repopulation of rotational states for C_2H^- prevents any modification of the thermal populations, other than uniform ion losses from all the levels populated in the traps.

A more telling effect on the selective population of rotational states for C_2H^- is shown by the simulation presented in the panels of Fig. 18. The data in the upper panel of that figure clearly show thermalization of the anion at 5 K after 5 s, when most of the molecular ions are in the $j = 1$ and $j = 2$ rotational states. As

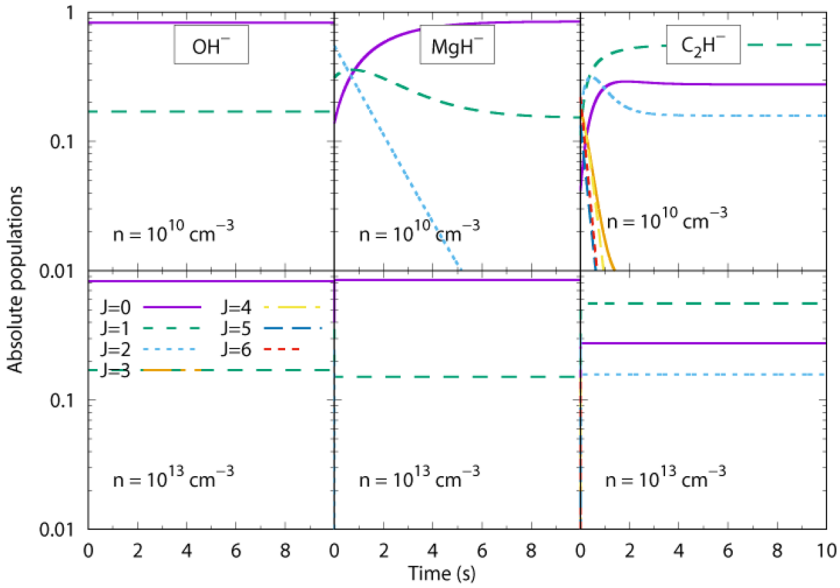

FIG. 16. Same calculations as those of Fig. 15 but at a lower trap temperature of 5 K. See main text for further details.

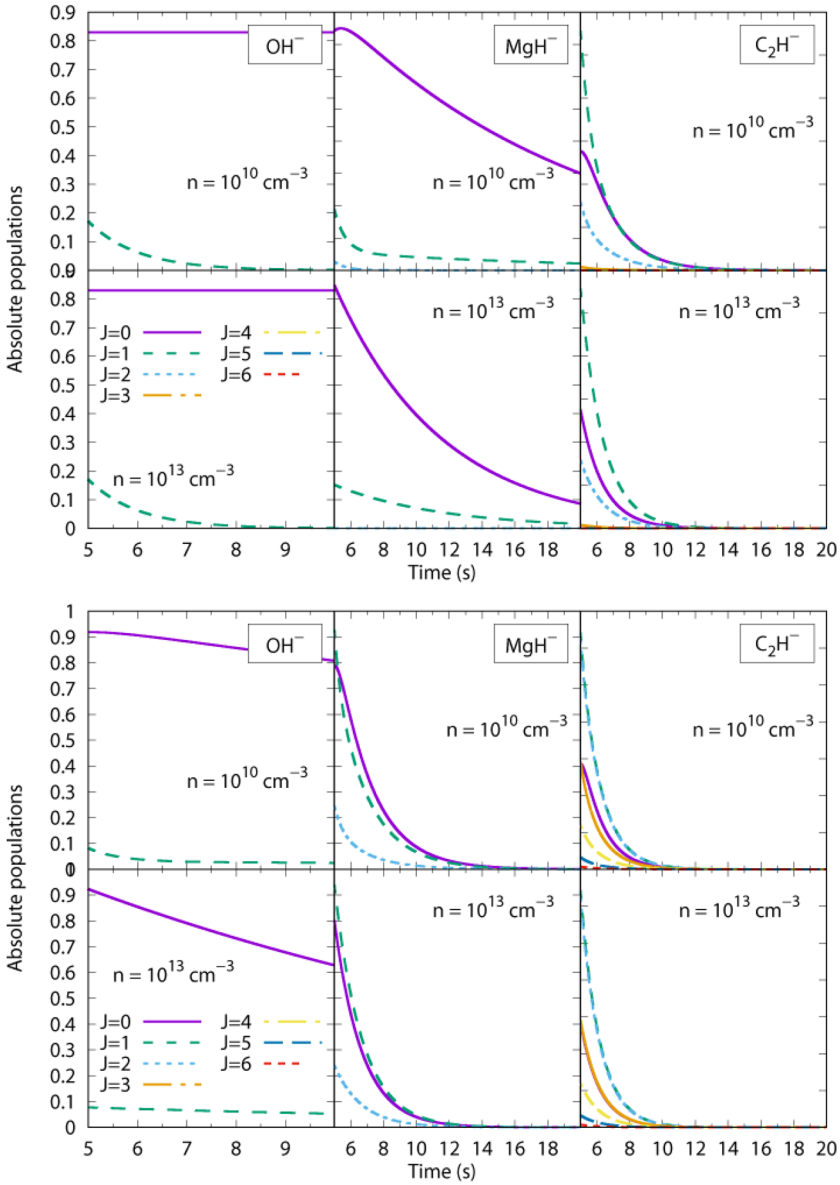

FIG. 17. Computed PD process with a fixed K^{PD} value of 1.0 s^{-1}. Upper panels at T = 5 K; lower panels at T'= 15 K. The laser is switched on after a 5 s delay, by which time all populations are thermalized to the buffer gas temperature.

the laser is switched on, we see losses from these two levels without any selective dominance of any of the anion's states. Due to the efficient collisional repopulation, the j = 1 and j = 2 levels are depleted very fast with the j = 0 level being the slowest. On the other hand, when the laser is selectively depleting from the j = 2 level as shown in the lower panel, we see that collisional repopulation is not sufficiently fast and it is possible to obtain a dominance of anions' population in the trap by the j = 1 rotational state: an example of the selective PD process coupled with collisional repopulation of the levels that are not directly depleted by the PD laser action.

To gauge the selective effects of changing the intensity of the PD laser, we repeat in the four sets of panels in Fig. 19 the calculations where the K^{PD} values are changed from 0.1 s^{-1} to 10.0 s^{-1} and where the laser frequency is "tuned" to deplete specific rotational levels of the anion. All cases in the figure refer to C_2H^-. The panels in Fig. 19 represent several numerical experiments of the PD process. Their behavior clearly indicates that, for K^{PD} = 0.1 and 0.5 s^{-1}, the photodetachment evolutions are collision-dominated and, for selecting the PD action only from the excited rotational states, the collisional repopulation keeps the populations nearly constant among all the lower levels reported in the upper two sets of panels. As the laser power is increased, however, we see that all levels indicate repopulation losses and we move into the PD-dominated regimes. It is also interesting to note that PD selective processes from the j = 3 level reveal how collisional repopulation produces a clear dominance of

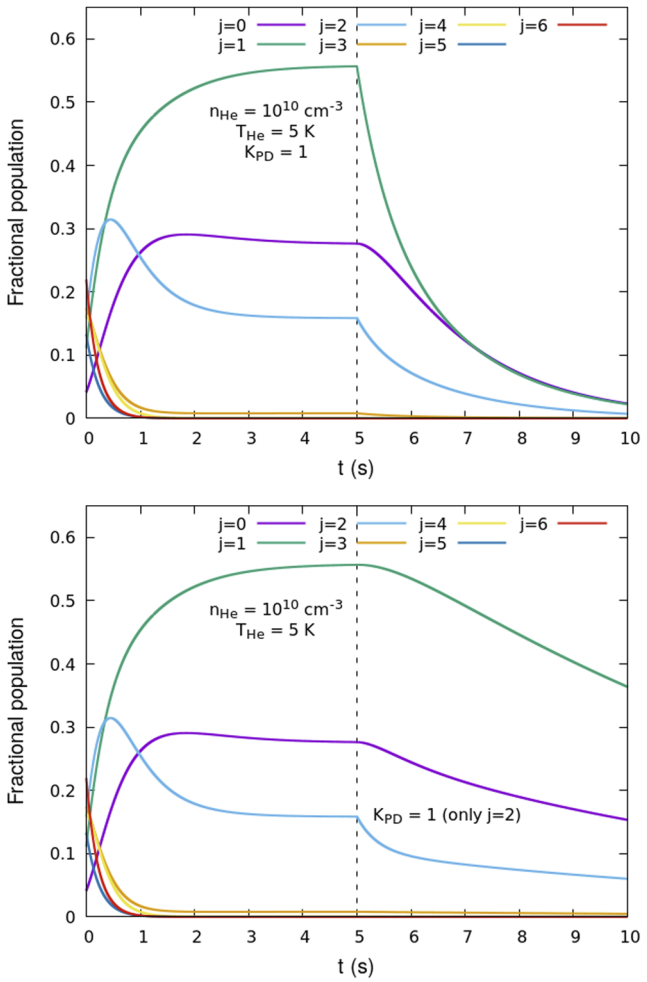

FIG. 18. Computed fractional populations for C_2H^- photodetachment processes. Upper panel: single K^{PD} = 1 s^{-1} "switched on" from all levels after 5 s. Lower panel: K^{PD} rate only photodetaching from the j = 2 level. See main text for further details.

j = 1 states of the C_2H^- anions, a feature that should be also amenable to experimental implementation and detection.

It is interesting to compare the efficient collisional repopulations between rotational levels of the C_2H^- anions with the behavior exhibited by the MgH^- anion, shown in the panels of the calculations reported by Fig. 20 for 15 K. It is worth being reminded that the strength of the laser power is kept here at K^{PD} = 1.0 s^{-1}. It corresponds to a laser intensity of medium value.[8,18] For C_2H^-, the populations of the j = 1 and j = 2 rotational states are the dominant ones: the efficient collisional repopulation processes occurring for this molecule essentially depopulate the upper j states, as well as the initial j = 0 state. Considering that the density of rotational states of MgH^- populated in the trap is lower than in the case of C_2H^- (see Fig. 1), we see that at 15 K both the j = 0 and j = 1 levels are equally the most populated after the PD laser is switched on, indicating a dominance of the collisional Boltzmann distributions.

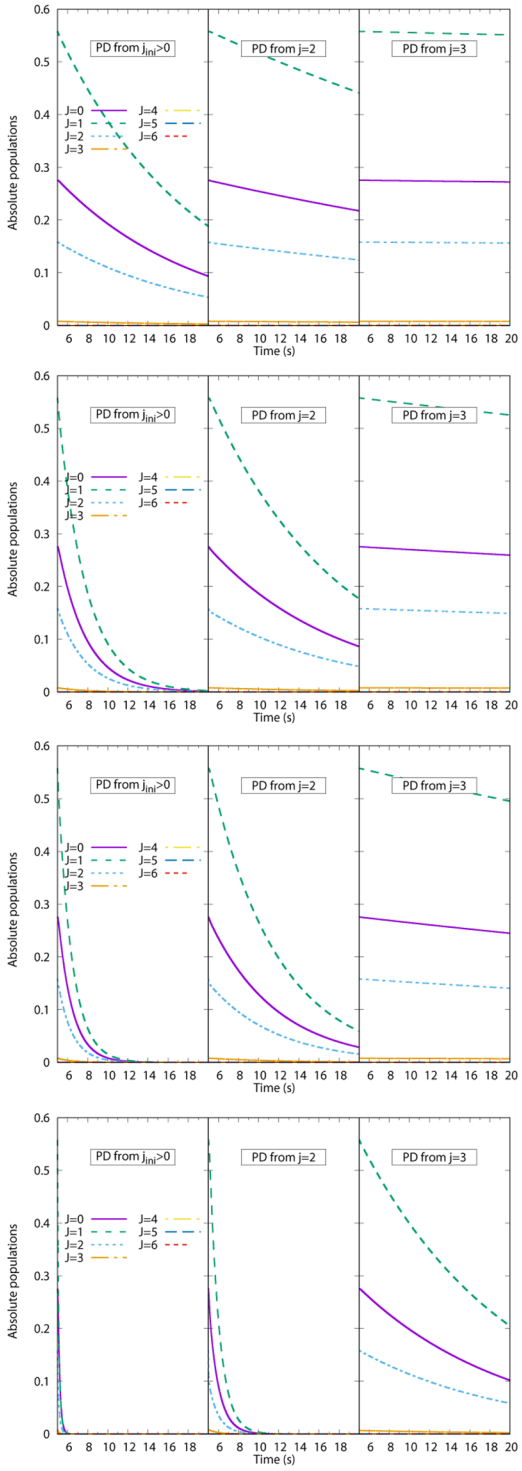

FIG. 19. Computed PD processes for C_2H^- using different strengths of the K^{PD} photodetachment rate: K^{PD} = 0.1 s^{-1} (top panels); K^{PD} = 0.5 s^{-1} (second row from top panels); K^{PD} = 1.0 s^{-1} (second row from bottom panels); K^{PD} = 10.0 s^{-1} (bottom panels). The trap temperature is T = 5 K, and the He density is 10^{11} cm^{-3}. See main text for further details.

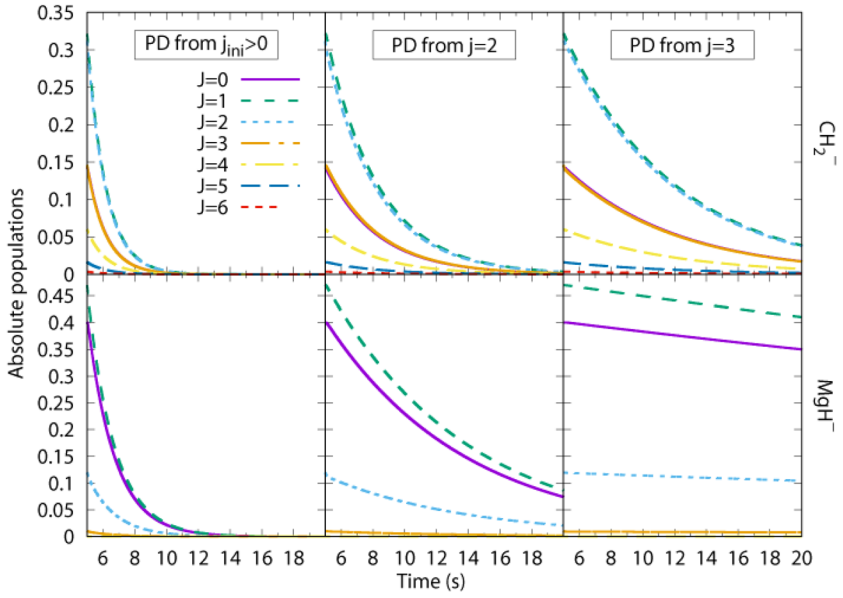

FIG. 20. Computed state-selective PD processes for C_2H^- (top panels) and MgH^- anions (bottom panels). Trap temperature of 15 K and η_{He} of 10^{11} cm^{-3}. The laser is "switched on" after 5 s of collisional thermalization in the trap after buffer gas uploading.

On the other hand, once the PD laser selectively depopulates higher rotational levels, for this anion a strong dominance of the $j = 0$ and $j = 1$ molecular population becomes possible. It therefore seems that also for this molecular anion the collisional repopulation of the lower rotational levels can produce in the trap an unbalanced population of states, which can further favor the dominance of the lower rotational levels.

VII. PRESENT CONCLUSIONS

In this work, we have analyzed the computational modeling of molecular photodetachment experiments involving small molecular anions confined in cold ion traps, with helium as the buffer gas of choice for the translational and internal cooling of molecules. We have selected three linear molecules in their ground electronic states, $OH^-(^1\Sigma)$, $MgH^-(^1\Sigma)$, and $C_2H^-(^1\Sigma)$, which are taken to be already cooled down to their ground vibrational levels and further thermalized to different rotational temperatures, the latter being reached in the trap by the presence of He as the buffer gas. We have considered trap temperatures from 5 to 20 K and selected buffer gas densities from 10^{10} to 10^{13} cm^{-3} in order to model different collision frequencies at which the trapped molecules undergo thermalization. We have further considered a broad range of laser powers by varying the PD rates from 0.1 up to 10.0 s^{-1}, thus covering several possible experimental setups, as seen, for instance, in Refs. 8 and 18. To simplify the present analysis of changing trap conditions, the modeled PD rates used in all the previous numerical tests have not been considered to be explicitly dependent on the initial rotational state of the anion but simply as constant quantities for each level from which the PD process is initiated. We shall analyze in later work the possible role of explicitly introducing the Hoenl-London factors and will show that their effects are decidedly less important than the parameter changes we discuss in the present work. Additionally, we have further modeled the state-selecting PD processes by making the K^{PD} rates as acting, within the nanoscopic dynamics, on different initial rotational levels of the selected anions during the trap kinetics.

To show the effects of the changing number of rotational levels populated in the trap, we have moved from OH^-, where only the $j = 0$ and $j = 1$ rotational states are significantly populated, to MgH^-, where at least three different rotational levels are actively populated, and then further considered the C_2H^- molecular anions, for which at least six different rotational states are actively interacting under trap conditions.

We have taken advantage of our knowledge of interaction forces between the He buffer gas and each of the molecular anions (which we had obtained in our earlier work from accurate *ab initio* quantum calculations) to first calculate the collisionally inelastic, state-changing cross sections involving the populated rotational levels of each different molecule in the trap. From such quantities, we have then obtained the corresponding state-changing collisional rates, $k_{i\to j}(T)$, and employed them within the kinetic analysis of the time-dependent population changes in the trap under different choices of trap parameters, e.g., temperature and buffer gas pressure, starting from different initial T values to model the collisional thermalization step for each of the molecules.

After reaching rotational state thermal distribution for different choices of trap parameters, we have "switched on" the PD laser action by selecting different values of the K^{PD} rates (related to the PD cross sections for the considered processes) and by making the presence of the K^{PD} rates as occurring only from selected initial rotational levels of the molecular anions. Here, we have only examined the selecting effects for the MgH^- and C_2H^- anions.

It is interesting to note at this point that recent simulation work of such processes in traps[32] analyzed the possible effects from the additional dynamics introduced by the presence of the RF field in

the trap. The micromotion interruptions induced by collisions of the ions with buffer-gas particles can in principle, and possibly also in practice, alter in a marked way the ion energy distribution and therefore affect the stabilized rotational populations of the trapped ion. The conditions of operation we are considering here seem to be, according to that study, still outside the range of the bifurcation effects on the ion energies, thereby reducing the importance of such processes in our modeling. In multipole ion traps, however, the micromotion interruptions induced by collisions of the ions with buffer-gas particles only slightly modify the rotational temperature at buffer gas temperatures above 20 K.[33] In any event, the additional quantum modelings of such effects while considering state-selective PD processes are at the moment outside the scope of the present work.

The calculations have allowed us to clearly see the consequences on state populations when moving from PD-dominated parameters in the trap to collision-dominated parameters for all three molecular systems. We have also been able to show that by making the PD rates as selectively acting only on a specific range of initial rotational levels, one can obtain anions in traps which have a marked non-Boltzmann distribution in their lower rotational levels and could therefore be prepared as having a detectable dominance of rotational state populations other than that of the $j = 0$ state.

The present work already shows that it is possible to carry out numerical modeling of specific outcomes from molecular PD experiments by "tuning" different physical parameters that describe trap conditions during that experiment.

ACKNOWLEDGMENTS

We are grateful to Professor Senent for kindly sending us their calculated multipolar coefficients for the C_2H^-–He system, which we have employed for our present calculations of state-changing cross sections and rates. We further acknowledge the financial support from the Austrian Science Fund (FWF) through Project No. P29558-N36. One of us (L.G.-S.) further thanks MINECO (Spain) for Grant Nos. CTQ2015-65033-P and PGD2018-096444-B-100.

REFERENCES

[1]F. Wolf, Y. Wan, J. C. Heip, F. Gebert, C. Shi, and P. O. Schmidt, "Non-destructive state detection for quantum logic spectroscopy of molecular ions," Nature **530**, 457 (2016).

[2]J. Biesheuvel, J.-P. Karr, L. Hilico, K. Eikema, W. Ubachs, and J. Koelemeij, "Probing QED and fundamental constants through laser spectroscopy of vibrational transitions in HD^+," Nat. Commun. **7**, 10385 (2016).

[3]W. B. Cairncross, D. N. Gresh, M. Grau, K. C. Cossel, T. S. Roussy, Y. Ni, Y. Zhou, J. Ye, and E. A. Cornell, "Precision measurement of the electron's electric dipole moment using trapped molecular ions," Phys. Rev. Lett. **119**, 153001 (2017).

[4]A. Kilaj, H. Gao, D. Rosch, U. Rivero, J. Kuepper, and S. Willitsch, "Observation of different reactivities of para and ortho-water towards trapped diazenylium ions," Nat. Commun. **9**, 2096 (2018).

[5]P. Puri, M. Mills, I. Simbotinl, J. A. Montgomery, Jr., R. Cote, C. Schneider, A. G. Suits, and E. R. Hudson, "Reaction blockading in a reaction between an excited atom and a charged molecule at low collision energy," Nat. Chem. **11**, 615 (2019).

[6]P. Jusko, M. Toepfer, H. S. P. Mueller, P. N. Ghosh, S. Schlemmer, and O. Asvany, "Double resonance rotational action spectroscopy of cold H_2D^+ and D_2H^+," J. Mol. Spectrosc. **332**, 33 (2017).

[7]T. D. Tran, S. Rednyk, A. Kovalenko, S. Roucka, P. Dohnal, R. Plasil, D. Gerlich, and J. Glosik, "Formation of H_2O^+ and H_3O^+ cations in reactions of OH^+ and H_2O^+ with H_2: Experimental studies of the reaction rate coefficients from T = 15 to 300 K," Astrophys. J. **854**, 25 (2018).

[8]O. Lakhmanskaya, M. Simpson, S. Murauer, M. Nötzold, E. Endres, V. Kokoouline, and R. Wester, "Rotational spectroscopy of a triatomic molecular anion," Phys. Rev. Lett. **120**, 253003 (2018).

[9]F. H. J. Hall and S. Willitsch, "Millikelvin reactive collisions between sympathetically cooled molecular ions and laser-cooled atoms in an ion-atom hybrid trap," Phys. Rev. Lett. **109**, 233202 (2012).

[10]D. Gerlich, "Ion-neutral collisions in a 22-pole trap at very low energies," Phys. Scr. **T59**, 256 (1995).

[11]P. F. Staanum, K. Højbjerre, P. S. Skyt, A. K. Hansen, and M. Drewsen, "Rotational laser cooling of vibrationally and translationally cold molecular ions," Nat. Phys. **6**, 271 (2010).

[12]T. Schneider, B. Roth, H. Duncker, I. Ernsting, and S. Schiller, "All-optical preparation of molecular ions in the rovibrational ground state," Nat. Phys. **6**, 275 (2010).

[13]D. Hauser, S. Lee, F. Carelli, S. Spieler, O. Lakhmanskaya, E. S. Endres, S. S. Kumar, F. Gianturco, and R. Wester, "Rotational state-changing cold collisions of hydroxyl ions with helium," Nat. Phys. **11**, 467–470 (2015).

[14]R. Wester, "Radiofrequency multipole traps: Tools for spectroscopy and dynamics of cold molecular ions," J. Phys. B: At., Mol. Opt. Phys. **42**, 154001 (2009).

[15]A. K. Hansen, O. O. Versolato, L. Kłosowski, S. B. Kristensen, A. Gingell, M. Schwarz, J. Windberger, J. R. Ullrich, C. López-Urrutia, and M. Drewsen, "Efficient rotational cooling of coulomb-crystallized molecular ions by a helium buffer gas," Nature **508**, 76 (2014).

[16]L. González-Sánchez, F. A. Gianturco, F. Carelli, and R. Wester, "Computing rotational energy transfers of OD^-/OH^- in collisions with Rb: Isotopic effects and inelastic rates at cold ion-trap conditions," New J. Phys. **17**, 123003 (2015).

[17]J. Xie and R. N. Zare, "Selection rules for the photoionization of diatomic molecules," J. Chem. Phys. **93**, 3033 (1990).

[18]O. Lakhmanskaya, M. Simpson, S. Murauer, V. Kokoouline, and R. Wester, "Photodetachment spectroscopy of cold trapped nh_2^- near threshold," J. Chem. Phys. **149**, 104302 (2018).

[19]L. González-Sánchez, F. Marinetti, E. Bodo, and F. A. Gianturco, "$Oh^-(x^1\sigma^+)$ collisions with $^4he(^1s)$ at vanishing energies: A quantum analysis of rotational quenching efficiency," J. Phys. B: At., Mol. Opt. Phys. **39**, S1203 (2006).

[20]L. González-Sánchez, S. Gómez-Carrasco, A. M. Santadaría, F. A. Gianturco, and R. Wester, "Investigating the electronic properties and structural features of MgH and of MgH^- anions," Phys. Rev. A **96**, 042501 (2017).

[21]F. Dumouchel, A. Spielfiedel, M. Senent, and N. Feautrier, "Temperature dependence of rotational excitation rate coefficients of C_2H^- in collision with He," Chem. Phys. Lett. **533**, 6 (2012).

[22]L. González-Sánchez, S. Gómez-Carrasco, A. M. Santadaría, R. Wester, and F. A. Gianturco, "Collisional quantum dynamics for MgH^- $(^1\sigma^+)$ with he as a buffer gas: Ionic state-changing reactions in cold traps," Front. Chem. **7**, 64 (2019).

[23]A. M. Arthurs and A. Dalgarno, "The theory of scattering by a rigid rotator," Proc. R. Soc. London, Ser. A **256**, 540 (1960).

[24]D. López-Durán, E. Bodo, and F. A. Gianturco, "Aspin: An all spin scattering code for atom-molecule rovibrationally inelastic cross sections," Comput. Phys. Commun. **179**, 821 (2008).

[25]R. Martinazzo, E. Bodo, and F. A. Gianturco, "A modified variable-phase algorithm for multichannel scattering with long-range potentials," Comput. Phys. Commun. **151**, 187 (2003).

[26]L. González-Sánchez, F. A. Gianturco, and R. Wester, "State-changing processes for ions in cold traps: LiH^- molecules colliding with he as a buffer gas," J. Phys. B: At., Mol. Opt. Phys. **49**, 235201 (2016).

[27]M. Hernández Vera, F. A. Gianturco, R. Wester, H. da Silva, O. Dulieu, and S. Schiller, "Rotationally inelastic collisions of H_2^+ ions with he buffer gas: Computing cross sections and rates," J. Chem. Phys. **146**, 124310 (2017).

[28]J. M. Brown and A. Carrington, *Rotational Spectroscopy of Diatomic Molecules* (Cambridge University Press, Cambridge, 2003).

[29]S. Brünken, C. A. Gottlieb, H. Gupta, M. C. McCarthy, and P. Thaddeus, "Laboratory detection of the negative molecular ion CCH^-," Astron. Astrophys. **464**, L33 (2007).
[30]C. Meyer, A. Becker, K. Blaum, C. Breitenfeldt, S. George, J. Göck, M. Grieser, F. Grussie, E. A. Guerin, R. von Hahn, P. Herwig, C. Krantz, H. Kreckel, J. Lion, S. Lohmann, P. M. Mishra, O. Novotný, A. P. O'Connor, R. Repnow, S. Saurabh, D. Schwalm, L. Schweikhard, K. Spruck, S. Sunil Kumar, S. Vogel, and A. Wolf, "Radiative rotational lifetimes and state-resolved relative detachment cross sections from photodetachment thermometry of molecular anions in a cryogenic storage ring," Phys. Rev. Lett. **119**, 023202 (2017).
[31]F. A. Gianturco, O. Y. Lakhmanskaya, M. Hernández Vera, R. Yurtsever, and R. Wester, "Collisional relaxation kinetics for *ortho* and *para* NH_2^- under photodetachment in cold ion traps," Faraday Discuss. **212**, 117–135 (2018).
[32]S. J. Schowalter, J. Dunning, A. K. Chen, P. Puri, C. Schneider, and E. R. Hudson, "Blue-sky bifurcation of ion energies and the limits of neutral-gas sympathetic cooling of trapped ions," Nat. Commun. **7**, 12448 (2016).
[33]S. S. Endres, S. Egger, G. Lee, O. Lakhmanskaya, M. Simpson, and R. Wester, "Incomplete rotational cooling in a 22-pole ion trap," J. Mol. Spectrosc. **332**, 134 (2017).